Hindawi
Journal of Nanomaterials
Volume 2022, Article ID 1967606, 19 pages
https://doi.org/10.1155/2022/1967606

Research Article

Application of Factorial Design and Response Surface Methodology in the Optimization of Clindamycin Nanocomposites

Yousef Rezek Almahamid,[1] Samer Hasan Hussein-Al-Ali,[1] and Mike Kh. Haddad[2]

[1]*Department of Basic Pharmaceutical Sciences, Faculty of Pharmacy, Isra University, P.O. Box 22, Amman 11622, Jordan*
[2]*Department of Renewable Energy Engineering, Faculty of Engineering, Isra University, P.O. Box 22, Amman 11622, Jordan*

Correspondence should be addressed to Samer Hasan Hussein-Al-Ali; sameralali72@yahoo.com

Received 22 February 2022; Accepted 27 July 2022; Published 31 August 2022

Academic Editor: Isaac Acquah

This study is aimed at achieving the optimized preparation of a new extended-release formulation of clindamycin (CLD) via loading of the CLD onto chitosan-chondroitin sulfate (CS-Chondro). The CS-Chondro-CLD nanocomposites were prepared by mixing different masses of CS (50, 100, and 200 mg) with Chondro (50, 100, and 200 mg) and different masses of CLD (75, 150, and 300 mg). The prepared nanocomposites were characterized by different techniques including loading efficiency (LE), X-ray powder diffraction (XRD), scanning electron microscopy (SEM), Fourier-transform infrared spectroscopy (FTIR), and release study. The XRD spectra of CS-Chondro-CLD nanocomposites showed two peaks at $2\theta = 22.5^{\circ}$ and 40.7°, indicating amorphous forms. The FTIR data shows incorporation of CLD into the CS-Chondro polymers. An *in vitro* release study of CLD from nanocomposites was carried out using PBS at pH 7.4. The result showed that the release rate was completed after 25 hours. This study showed that the CS-Chondro-CLD nanocomposites have promising applications in the delivery of CLD drug.

1. Introduction

A new advanced topic in pharmaceutical studies known as "pharmaceutical nanotechnology" focuses on pharmaceutical development. Nanoparticles are solid colloidal particles ranging in size from 10 nm to 1 μm [1]. The physical and chemical properties of materials change when prepared in nanoscale, leading to a noticeably different surface chemistry of nanoparticles compared to that of the original material [2, 3]. Major advantages of nanoparticles include increased rate of dissolution, solubility, oral bioavailability, therapeutic action, and lower amount of dose required [4].

Nanotechnology and nanoparticles are helping to considerably improve many technologies and industries such as information technology, photocatalytic applications, medicine, energy, food safety, and environmental sciences [5–8].

Polymeric nanoparticles are popular due to their ease in preparation with required characteristics for drug delivery systems. They provide an intelligent alternative for the conventional dosage form of therapeutic agents for chronic administration [9]. In addition, nanoparticles protect loaded bioactive substances against degeneration by enzymes [10]. Polymeric nanoparticles were used to overcome gastrointestinal challenge by interaction between the drug and epithelial cells in the gastrointestinal tract [11].

Chondroitin sulfate is a water-soluble component of cells, tissues, and organs. It is a major constituent of the extracellular structure [12, 13].

Chondroitin and other polymers such as albumin and chitosan have been a material of choice for the delivery of oligonucleotides, DNA, protein, and drugs [14, 15]. Chondroitin sulfate in tissues undergoes natural conversion in the physiological environment to provide controlled release of the drug [16]. The reaction of chondroitin with the drug to obtain the novel substances is carried out in a manner dependent on the functional groups involved. Chondroitin

is the most extensively studied encapsulating material for the controlled release of drugs [16].

Clindamycin (CLD) drug was approved by the US Food and Drug Administration for treatment of anaerobic infections. It is used alone or in combination with other therapies for treating several cases such as infections of the head and neck, respiratory system, babesiosis which causes flow out of red or blackish urine, acne vulgaris, vagina, bone and soft tissue, and abdomen. CLD can be bactericidal or bacteriostatic depending on its concentration and site of infection [17]. Common side effects of CLD use include rash and diarrhea which could be resolved through a strategy to prevent antibiotic-associated diarrhea and mainly probiotic administration for short time [18]. In spite of the comparatively short half-life of CLD, in which it is administered every 8 hours for 5-7 days, it is considered an appropriate treatment for most contagions. In patients with normal renal function, the half-life is 2.4 hours [19].

Clindamycin was used as a hydrophilic cationic drug loaded with dextran sulphate or sodium alginate as an anionic polymer. The results showed that these properties for polymers had a significant effect on drug loading, as the presence of dextran sulphate increased from 1.32 to 18.19%, as well as an effect on reducing the release for the drug. This improved performance of CLD was due to the novel properties of small particle size and increase surface area [20].

An attempt to study the effect of transfersomal (TRSS) on the delivery of CLD through the skin showed an enhanced penetration of the drug. The characteristics of the particles such as entrapment efficiency, particle size, surface charge, and morphology were evaluated. TRSS showed higher entrapment efficiency (EE) of 93.3%, which led to a higher *in vitro* release of CLD [21].

Rauta et al. focused on increasing the efficacy of CLD loaded on PLA/PLGA polymer as novel nanoparticle delivery system by oral administration. The results confirmed that CLD-PLA/PLGA polymers significantly increased the bioavailability and drug activity [22].

In another study that prepared CLD-alginate and chitosan composites as mucoadhesive drug delivery system for periodontal therapy, the results showed that concentration of sodium alginate and the molecular weight of chitosan affected the characteristics of the composites such as thickness, encapsulation, structure, tumescence, adhesion, and *in vitro* drug release [23].

The aim of the present study is to prepare a novel nanocomposite, which contains CLD loaded onto chitosan-chondroitin to enhance the release properties.

2. Experimental

2.1. Materials. The chemicals used in this study are clindamycin hydrochloride monohydrate ($C_{18}H_{34}Cl_2N_2O_5S.H_2O$, Sigma-Aldrich), low molecular weight chitosan (10-120 kDa, Sigma-Aldrich), chondroitin sulphate ($C_{13}H_{21}NO_{15}S$, Sigma-Aldrich), and phosphate-buffered saline tablets (PBS) (Sigma-Aldrich). The acetic acid was purchased from Chem CO (England).

Table 1: Levels of CS, Chondro and CLD factors.

Factors	Unit	Low level	Middle level	High level
CS	mg	50	100	200
Chondro	mg	50	100	200
CLD	mg	75	150	300

2.2. Instrumentation. All the prepared samples (CS-Chondro and CS-Chondro-CLD) and standard CLD samples were studied using several instruments, which are detailed as follows:

(1) X-ray diffraction (XRD) was studied using CuK radiation at 30 kV and 30 mA (GBC Scientific Equipment, USA) at the Institute of Functional Nanosystems, UIM University (Germany)

(2) Fourier transform infrared spectroscopy (FTIR) data spectra were measured by a Thermo Nicolet Nexus, Smart Orbit spectrometer

(3) The scanning electron microscope (SEM) images were obtained at 10 kV, Hitachi High-Tech Global

(4) The UV-Vis spectra were measured using Shimadzu UV-1601

(5) Zeta potential and particle size of formulations were analyzed through dynamic light scattering (DLS) with Zetasizer Nano S (Malvern UK)

3. Methods

3.1. Design of Experiment. Full factorial design was used to study the %LE, zeta potential, and particle size as responses of the CS, Chondro and CLD preparations. The ranges of values used in the design are described in Table 1, and all the experimental run results are presented in Table 2.

3.2. Data Analysis of the Factorial Design. A plot of residuals versus corresponding predicted values, a response surface plot, a normal probability plot of the residuals, and interaction plots were used as graphical tools for the analysis of the factorial design.

A regression analysis was also used to study the relationship between the independent variables (CS, Chondro, and CLD) and the response (LE, size, and zeta potential). The experimental data were processed by using Minitab software version 18 [24].

3.3. Preparation of CS-Chondro Nanoparticles and CS-Chondro-CLD Nanocomposites. CS-Chondro nanoparticles were prepared by ionic gelation technique [25]. The CS (50, 100, 200 mg) was dissolved in 1% (*w*/*v*) acetic acid. Chondro solutions with masses of 50, 100, and 200 mg were added to CS solution, and the pH was controlled at 5, with stirring for 18 hours [26]. The product was collected at 11000 rpm.

CS-Chondro-CLD nanocomposites were formed by a drop-wise method of the aqueous solution of Chondro with

Table 2: Matrix for 3^3 full factorial designs.

Std. order	Sample code	CS	Chondro	CLD	%LE	Size	Potential
50	1	200	100	150	*	*	10.8
67	2	100	100	75	*	130	-14.3
69	3	100	100	300	71.3	181	*
22	4	200	100	75	31.3	*	*
63	5	50	200	300	75.2	*	-9.9
51	6	200	100	300	75.7	304	5.7
7	7	50	200	75	19.1	150	-7.6
47	8	200	50	150	52.2	*	14.9
16	9	100	200	75	6.3	*	-18.2
11	10	100	50	150	66.0	185	-8.4
38	11	100	50	150	62.7	*	-6.3
74	12	200	50	150	54.5	*	14.9
70	13	100	200	75	5.5	171	-18.6
42	14	100	100	300	68.5	244	*
40	15	100	100	75	*	150	-15.9
79	16	200	200	75	33.6	300	12.3
14	17	100	100	150	50.8	164	-7.3
2	18	50	50	150	*	176	-2.0
3	19	50	50	300	86.9	240	-6.2
43	20	100	200	75	7.8	190	-19.1
77	21	200	100	150	*	*	10.9
33	22	50	100	300	*	182	*
26	23	200	200	150	26.8	275	12.4
56	24	50	50	150	*	*	-6.4
61	25	50	200	75	15.2	111	-7.4
8	26	50	200	150	23.3	151	-8.5
71	27	100	200	150	22.2	152	-8.8
32	28	50	100	150	69.3	*	*
19	29	200	50	75	27.9	460	19.2
5	30	50	100	150	52.3	*	*
73	31	200	50	75	28.5	450	19.6
4	32	50	100	75	32.9	*	*
46	33	200	50	75	26.2	445	20.0
20	34	200	50	150	57.2	*	14.9
76	35	200	100	75	33.2	340	*
34	36	50	200	75	14.3	147	-7.8
27	37	200	200	300	71.1	200	13.4
25	38	200	200	75	23.8	297	12.0
58	39	50	100	75	36.2	*	*
60	40	50	100	300	*	180	*
75	41	200	50	300	71.5	308	8.0
53	42	200	200	150	30.5	252	12.4
24	43	200	100	300	78.0	*	3.6
72	44	100	200	300	56.0	261	-12.6
31	45	50	100	75	24.6	*	*

Table 2: Continued.

Std. order	Sample code	CS	Chondro	CLD	%LE	Size	Potential
12	46	100	50	300	64.8	*	-19.4
23	47	200	100	150	*	328	11.0
59	48	50	100	150	62.3	*	*
62	49	50	200	150	26.5	201	-7.8
6	50	50	100	300	*	185	*
64	51	100	50	75	*	177	-10.6
17	52	100	200	150	23.0	203	-18.7
55	53	50	50	75	60.5	*	-6.8
49	54	200	100	75	31.7	379	*
57	55	50	50	300	86.4	230	-6.1
45	56	100	200	300	58.0	225	-12.6
66	57	100	50	300	61.7	238	-18.9
80	58	200	200	150	34.9	302	12.3
1	59	50	50	75	61.4	*	-8.7
36	60	50	200	300	76.2	*	-7.9
44	61	100	200	150	23.6	206	-13.8
9	62	50	200	300	87.7	*	-5.9
30	63	50	50	300	88.4	244	-6.3
52	64	200	200	75	27.7	302	12.7
41	65	100	100	150	62.8	185	-10.3
78	66	200	100	300	79.9	298	7.8
15	67	100	100	300	72.2	*	*
68	68	100	100	150	60.1	150	-8.8
54	69	200	200	300	75.0	192	14.2
28	70	50	50	75	61.0	*	-7.7
37	71	100	50	75	*	158	-11.4
81	72	200	200	300	74.0	191	12.6
29	73	50	50	150	*	*	-7.2
48	74	200	50	300	71.0	*	8.6
13	75	100	100	75	*	132	-17.5
21	76	200	50	300	76.3	303	7.5
65	77	100	50	150	*	150	-10.5
39	78	100	50	300	55.0	229	-18.4
10	79	100	50	75	*	149	-9.8
35	80	50	200	150	29.6	190	-9.1
18	81	100	200	300	55.5	250	-12.6

*The deleted sample during processing with data.

50, 100, and 200 mg into 50, 100, and 200 mg solution of CS, containing 75, 150, and 300 mg of CLD, with constant stirring. The resulting nanocomposites were collected by centrifugation at 11000 rpm [26].

3.4. The CLD Loading Efficiency. The procedure for calculating loading efficiency (%LE) was as follows: 2.0 ml of suspension was centrifuged at 11000 rpm; then the free drug was measured by UV-Vis at λ_{max} of 300 nm.

$$\%\text{LE} = \frac{Q_T - Q_{un}}{\text{mass of nanocomposite}} \times 100, \quad (1)$$

where Q_T is the total CLD used during preparation and Q_{un} is the free CLD in the supernatant.

3.5. In Vitro Release Study of CLD from CS-Chondro-CLD Nanocomposites. An in vitro release study of CLD from CS-Chondro-CLD nanocomposites was carried out in PBS

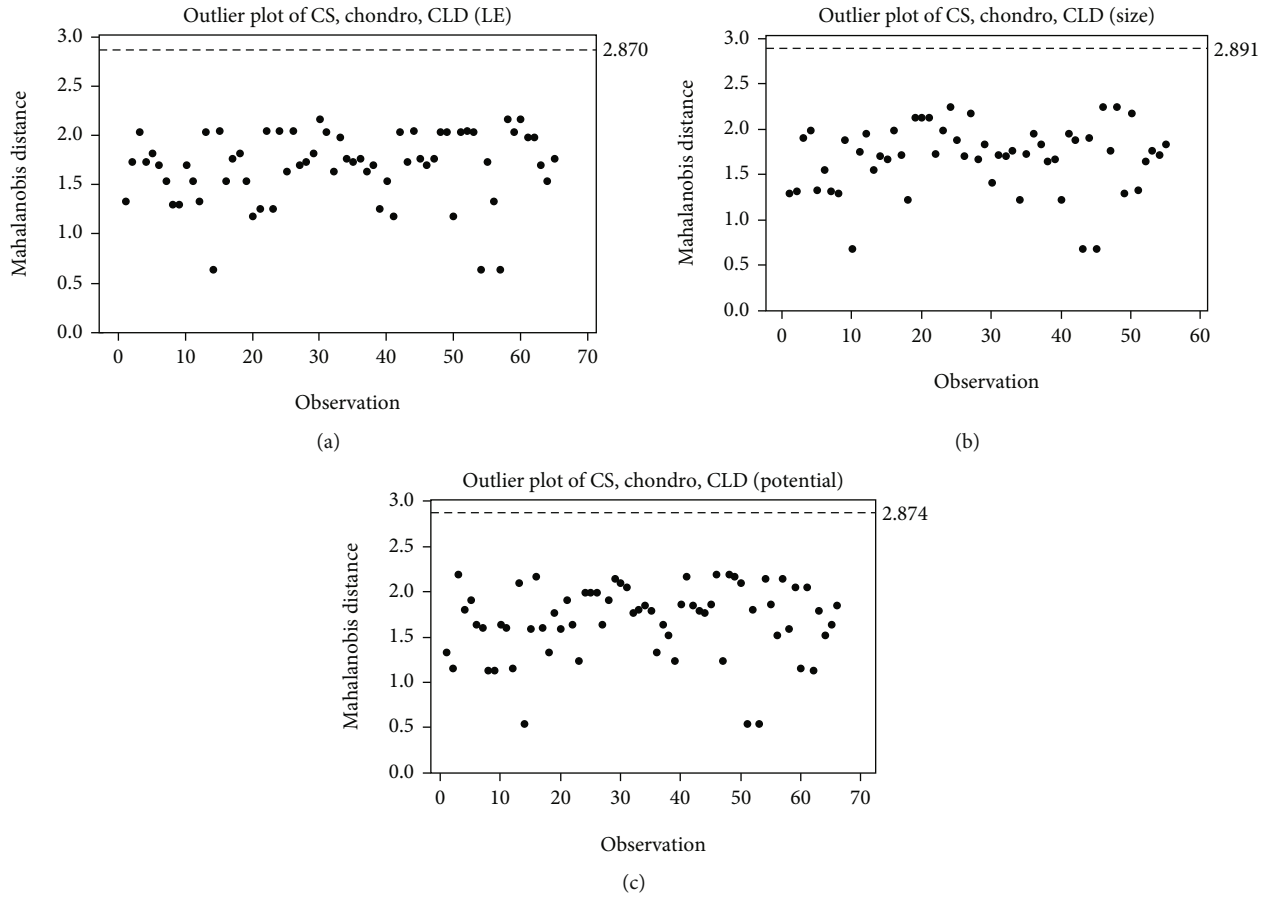

Figure 1: Dj model value for independent variables values for %LE (a), particle size (b), and zeta potential (c).

at pH 7.4, at λ_{max} of 300 nm. A suitable amount of nanocomposite was added to the release media. The cumulative amount of CLD released into the media was measured at different time intervals [27]. The percentage release of CLD was calculated using the following equation:

$$\%\text{Release} = \frac{\text{Concentration of CLD time } t}{\text{Concentration of CLD in the nano Formulations}} \times 100. \quad (2)$$

4. Results and Discussion

4.1. Detection Outlier Reading. An outlier is a reading which deviates from other data. For univariate data, familiar Euclidean distance and rarity are used in the data analysis, but for multivariate data, the Mahalanobis distance method was used. It enables detecting multivariate outliers that need to be eliminated from future analysis to enhance a model.

Mahalanobis distance (Dj) can be defined as the distance between a data point and overall mean. It is based on the vector of data (x) and the vector of mean values of independent variables (m) [28].

The formula used for Mahanabolis distance [29] is as follows:

$$Dj = (x - m)^T C^{-1} (x - m), \quad (3)$$

where T indicates the vector should be transposed and C^{-1} is the inverse covariance matrix of independent variables.

From the Dj standard formula, the values of the outliers are identified for the independent variables values which are dependent on the concentration of CS, Chondro, and CLD.

In the Dj value, threshold values are assigned to the multivariate data. The list of the threshold values assigned for different variants is given in Figure 1.

As in the current work, the critical value is for three independent variables (threshold is 2.858) (Figure 1(a)); the Dj values found above 2.858 are outliers. Fortunately, there are no outlier values suspected as spam to all responses. With regard to %LE, particle size, and zeta potential data analysis, the amount of data was deleted to increase the R^2 value. Therefore, the Dj values become 2.870 (%LE) (Figure 1(b)), 2.891 (particle size) (Figure 1(c)), and 2.874 (zeta potential) (Figure 1(d)), without any outlier values for all experiments being recorded.

Table 3: ANOVA data for %LE, particle size, and zeta potential models.

	LE model						Particle size model						Zeta potential model				
	t value	Coef	*F* value	*p* value	VIF		*t* value	Coef	*F* value	*p* value	VIF		*t* value	Coef	*F* value	*p* value	VIF
Model	19.83	44.23	72.61	0.00	—	Model	23.24		86.72	0.00		Model	-11.79	-12.47	164.29	0.00	
Linear	—	—	130.09	0.00	—	Linear			97.67	0.00		Linear			183.40	0.00	
CS	-2.57	-3.26	6.63	0.00	1.06	CS	16.54	71.43	273.56	0.00	1.16	CS	23.33	9.873	544.36	0.00	1.18
Chondro	-7.95	-9.68	63.28	0.00	1.02	Chondro	-4.39	-17.42	19.26	0.00	1.15	Chondro	-1.87	-0.666	3.48	0.00	1.04
CLD	17.35	21.82	300.85	0.00	1.05	CLD	2.87	11.27	8.23	0.00	1.12	CLD	-2.71	-1.099	7.33	0.00	1.06
Square			14.46	0.00	—	Square			16.36	0.00		Square			121.54	0.00	
CS* CS	3.80	10.22	14.46	0.00	1.11	CS* CS	3.52	27.91	12.38	0.00	1.20	CS* CS	17.94	14.371	321.76	0.00	1.14
Chondro* Chondro						Chondro* Chondro	4.08	33.78	16.67	0.00	1.10	Chondro* Chondro	2.34	2.37	5.49	0.00	1.17
CLD* CLD													-2.82	-2.184	7.95	0.00	1.07
2-way interaction	—	—	17.34	0.00	—	2-way interaction			97.75	0.00		2-way interaction			18.45	0.00	
CS* Chondro	4.13	5.84	17.07	0.00	1.00	CS* Chondro	-9.74	-48.29	94.77	0.00	1.18	CS* Chondro					
Chondro* CLD	4.34	6.18	18.83	0.00	1.02	Chondro* CLD						Chondro* CLD	5.17	-1.467	26.71	0.00	1.02
CS* CLD						CS* CLD	-12.5	-62.33	155.92	0.00	1.19	CS* CLD	-3.03	2.187	9.16	0.00	1.05

Table 4: K-S and A-P tests for goodness-of-fit models.

	%LE model	Particle size model	Zeta potential model
D_n (calculated value for K-S test)	0.143	0.156	0.107
D_{crit} (critical value for K-S test)	0.170	0.183	0.167
$D_{Agostino\text{-}Pearson}$ (A-P test)	0.084	0.006	0.072

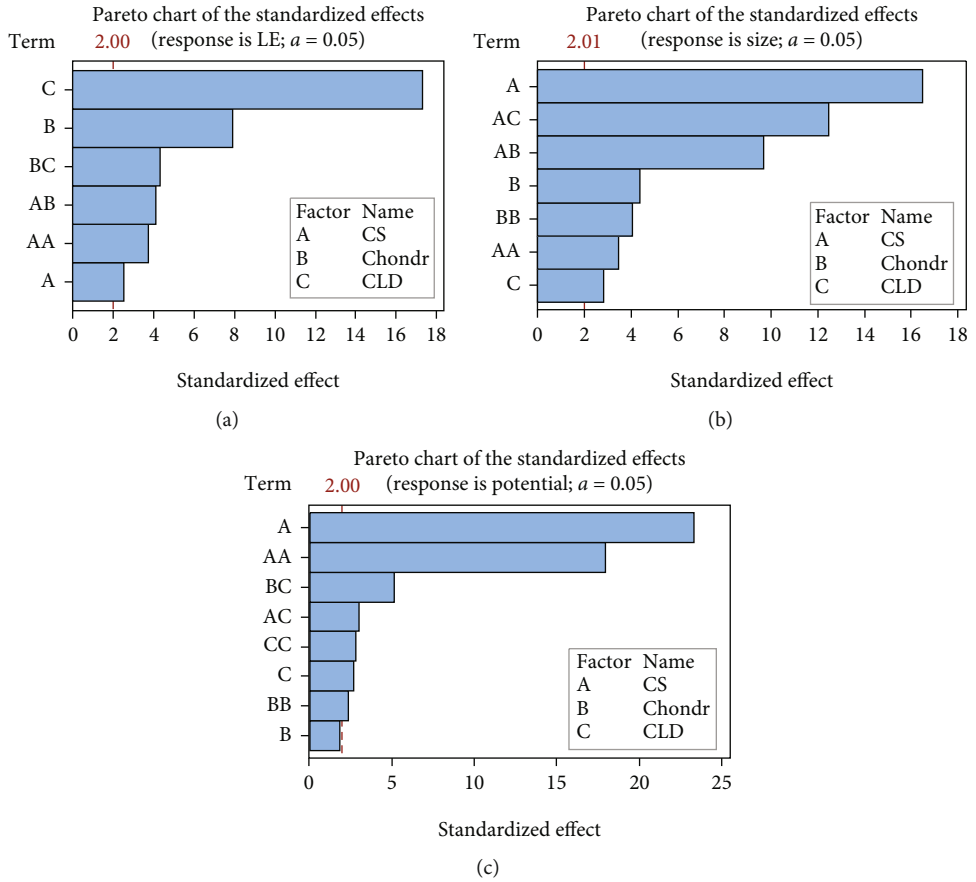

Figure 2: Pareto chart of the %LE (a), particle size (b), and zeta potential (c).

4.2. Statistical Data Analysis. The variance inflation factor (VIF) is one of the methods used to assess the multicollinearity properties, i.e., if the predictors are correlated. If no factors are correlated, the VIFs will all be <5 [30]. Due to absence of multicollinearity in this work, the data was analyzed using the multivariate regression model.

Multiple regressions is a method used to predict the value of a variable based on the value of two or more other variables [31].

4.2.1. ANOVA Data. From ANOVA data for the %LE model in Table 3, we estimated the individual factors (CS, Chondro and CLD) and their combinations on the response (CS ∗ CS, CS ∗ Chondro, and Chondro ∗ CLD). The significant effect on the %LE can be seen with a p value less than 0.05 and a high F value. From Table 3, we noted the following important characteristics: (i) the average p value for the model, individual factors, and their combinations are much less than 0.05, which means that the conditions in the model have a high significance [32]; (ii) the F values for individual factors (CLD, Chondro, and CS) were 300.85, 63.28, and 6.63, respectively, whereas the F value for combinations (Chondro ∗ CLD, CS ∗ Chondro, and CS ∗ CS) was 18.83, 17.07, and 14.46, respectively.

Table 3 shows ANOVA data for the particle size model. The results of the statistical evaluation and variance analysis of the data show that all of the variables and their interactions had significant effects except CLD ∗ CLD and CLD ∗ Chondro. Also, the F value of the model was 86.72; this large value could occur due to noise [33, 34].

Table 3 also shows the F value and p value for zeta potential model. From the data in Table 3, the F values for individual factors (CLD, Chondro, and CS) were 7.33, 3.48, and 544.36, respectively, whereas the F value for combinations

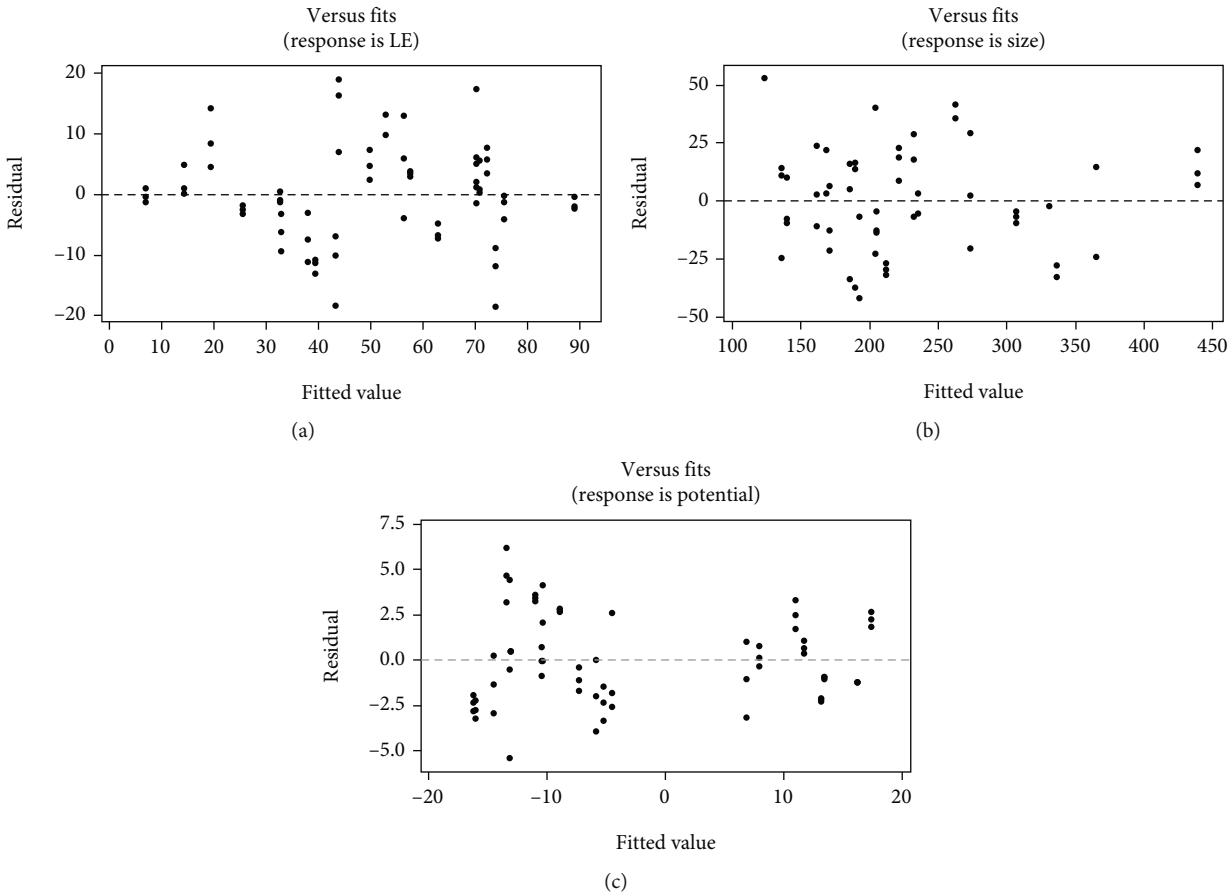

Figure 3: The residuals plot versus the fitted values for %LE (a), particle size (b), and zeta potential (c).

(CS ∗ CS, Chondro ∗ Chondro, CLD ∗ CLD, Chondro ∗ CLD, and CS ∗ CLD) was 321.76, 5.49, 7.95, 26.71, and 9.16, respectively.

In statistics, the coefficient of determination (R^2) is the proportion of the variation in the dependent variable which is predictable from the independent variable(s). The R^2 for the %LE model was 88.25%, and the R^2_{adj} is 87.04%. In addition, the value of R^2 for particle size model was 92.81%, and the R^2_{adj} is 91.74%. Finally, the R^2 for the zeta potential model was 95.84%, and the R^2_{adj} is 95.26%. There is no difference between the R^2 and R^2_{adj} values, which indicate the significant conditions in the three models.

4.3. Goodness-Of-Fit Test for the Normal Distribution for Three Models

4.3.1. The Kolmogorov-Smirnov (K-S) Test for Goodness-Of-Fit. The K-S test is a nonparametric test of the equality of continuity, and it contains one and two samples. At the one-sample test, one-dimensional probability distributions are used to compare a sample with a reference probability distribution (hypothesized distribution), whereas a two-sample test is one of the most useful and general nonparametric methods for comparing two samples [35, 36].

The K-S test null hypothesis is defined as [37] follows:

H_o: the sample data are not significantly different than a normal population.

H_a: the sample data are significantly different than a normal population.

The D_n calculated value can be determined by the following equation:

$$D_n = \max_{1\le i\le N}\left(F(Y_i) - \frac{i-1}{N}, \frac{i}{N} - F(Y_i)\right), \tag{4}$$

where F is the theoretical cumulative distribution.

The critical value of the K-S test can be calculated by the following equation [38]:

$$D_{\text{crit},0.05} = \frac{1.36}{\sqrt{n}}. \tag{5}$$

4.3.2. The D'Agostino-Pearson (A-P) Test. The D'Agostino-Pearson test is a very powerful test for assessing departures from normality [39]. The null hypothesis is defined as follows:

H_o: the sample data are not significantly different than a normal population.

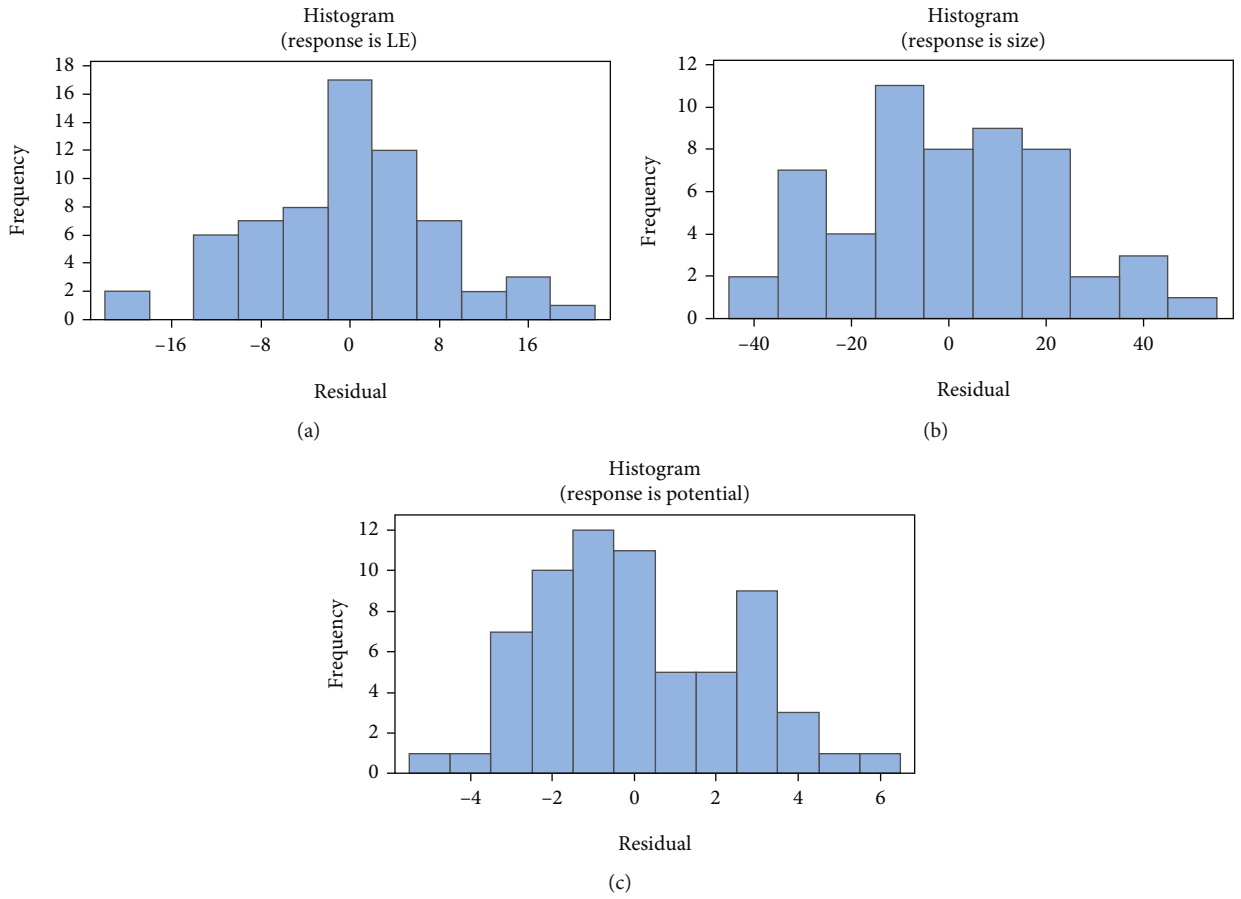

Figure 4: Histogram of the standardized residuals for %LE (a), particle size (b), and zeta potential (c).

H_a: the sample data are significantly different than a normal population.

The D is a test that can statistically calculate the value by the following equation:

$$D = \frac{T}{\sqrt{n^3 \mathrm{SS}}}, \tag{6}$$

where "SS" is the sum of squares of the data and "n" is the sample size.

$$T = \sum \left(i - \frac{n+1}{2} \right) X_i, \tag{7}$$

where "i" is the order or rank of observation.

From the results in Table 4, D_{crit} (critical value) for %LE, particle size, and zeta potential are bigger than D_n (calculated value); therefore, the null hypothesis is not rejected (for the normally distributed data). In addition, the $D_{\text{Agostino-Pearson}}$ value for %LE and zeta potential is bigger than 0.05 ($D > p$), indicating that the model set is not significantly different than normal.

4.4. Pareto Chart of the Standardized Effects of the Three Models. A Pareto chart is normally used as a graphical representation for evaluating the effects of the main variables and their interactions on the response. Figure 2 shows the bars of the main f variables and their interactions, arranged in a descending order according to the t values. The vertical line is the statistical threshold for a level of significance.

From the results in Figure 2(a), it can be seen that three main factors have a statistically significant effect on the %LE. In a descending order, according to their effect estimates, the three factors are CLD, Chondro, and CS, and the interactions Chondro ∗ CLD (BC), CS ∗ Chondro (AB), and CS ∗ CS (AA).

In addition, in the Pareto chart in Figure 2(b) which is related to particle size model, bars that cross the reference line (2.01) are statistically significant with the following order: A>AC>AB>B>BB>AA>C.

Figure 2(c) plots the effects in the decreasing order of their absolute values with reference line at 2 values calculated by Lenth's method [40]. In these results, the two main effects (CS and CLD) are statistically significant ($\alpha = 0.05$). In addition, the two square effects (CS ∗ CS (AA), Chondro ∗ Chondro (BB), and CLD ∗ CLD (CC)) are statistically significant ($\alpha = 0.05$). The two-way interaction (Chondro ∗ CLD (BC) and CS ∗ Chondro (AB)) can also be seen, which also shows significant results.

4.5. Residual Plot. Figure 3 shows the correlation between residuals with predicted responses of the three models. The

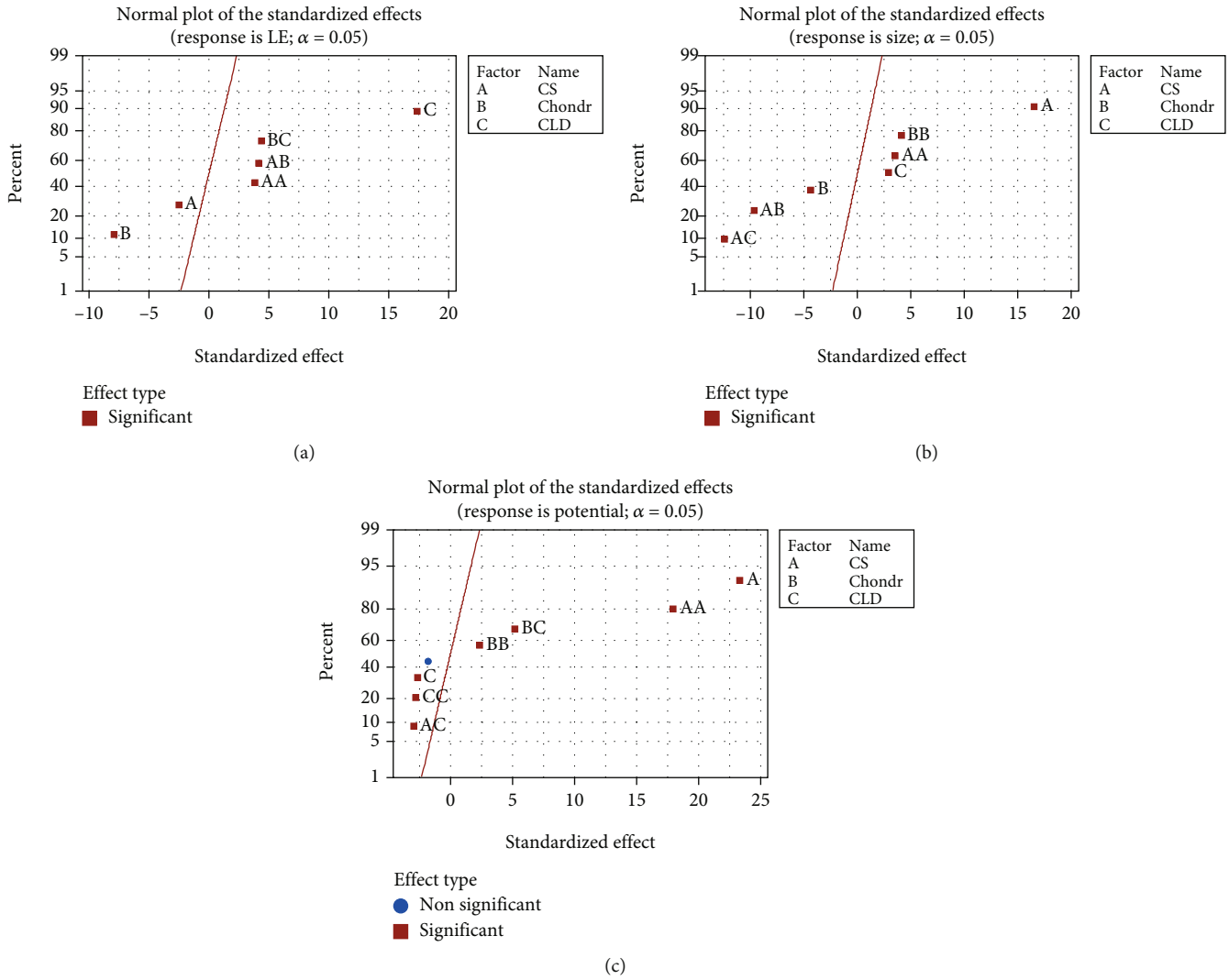

Figure 5: Normal probability plot of the effects for %LE (a), particle size (b), and zeta potential (c).

residuals of three models are scattered randomly about zero. These results indicate that the errors have a constant variance and the experiment does not contain any possibility of systematic errors.

4.6. Histogram Plot. The histogram plot of residuals are used to determine whether the data are skewed or outliers exist in the data. Figures 4(a)–4(c) show the %LE, particle size, and zeta potential histogram residual plots, respectively. Results show symmetric bell-shaped curves, indicating that the data are complete residual normality assumption.

4.7. Normal Probability Plot of the Standard Effects. Figures 5(a)–5(c) shows the normal probability plot of the effects for %LE, particle size, and zeta potential, respectively.

From Figure 5(a), it could be seen that there are no factors or combinations on a line which lies close to zero. Three of the individual factors show deviation of varying degrees—A and B (negative direction) and C (positive direction). In addition, three of the combinations at level two—AA, AB, and BC—showed a significant result toward %LE response with positive direction. From Figure 5(b), it can be seen that three of the factors show negative direction (B, AB, and AC) and four of the factors show positive direction (A, C, AA, and BB). In addition, Figure 5(c) shows significant positive direction for A, AA, BB, and AB factors, whereas the factors C, CC, and AC show significant negative direction.

4.8. Contour Plot and Surface Plot of Responses against Different Factors. Figure 6(a) shows the contour plot of %LE. The %LE with a value higher than 60% corresponds with high values of CLD and Chondro, but varies from 50 mg to 200 mg, and the surface is maximum (Figure 6(b)).

Figure 6(c) shows the dependence of %LE on CS and CLD. When CS concentrations are at their minimum and maximum levels and at same time the CLD is at maximum level, the %LE was found to be maximum surface (Figure 6(d)). However, the contour of CS against Chondro concentrations (Figure 6(e)) showed the highest %LE in the lower left of the plot, which corresponds with low values of CS and Chondro, and the surface is maximum (Figure 6(f)).

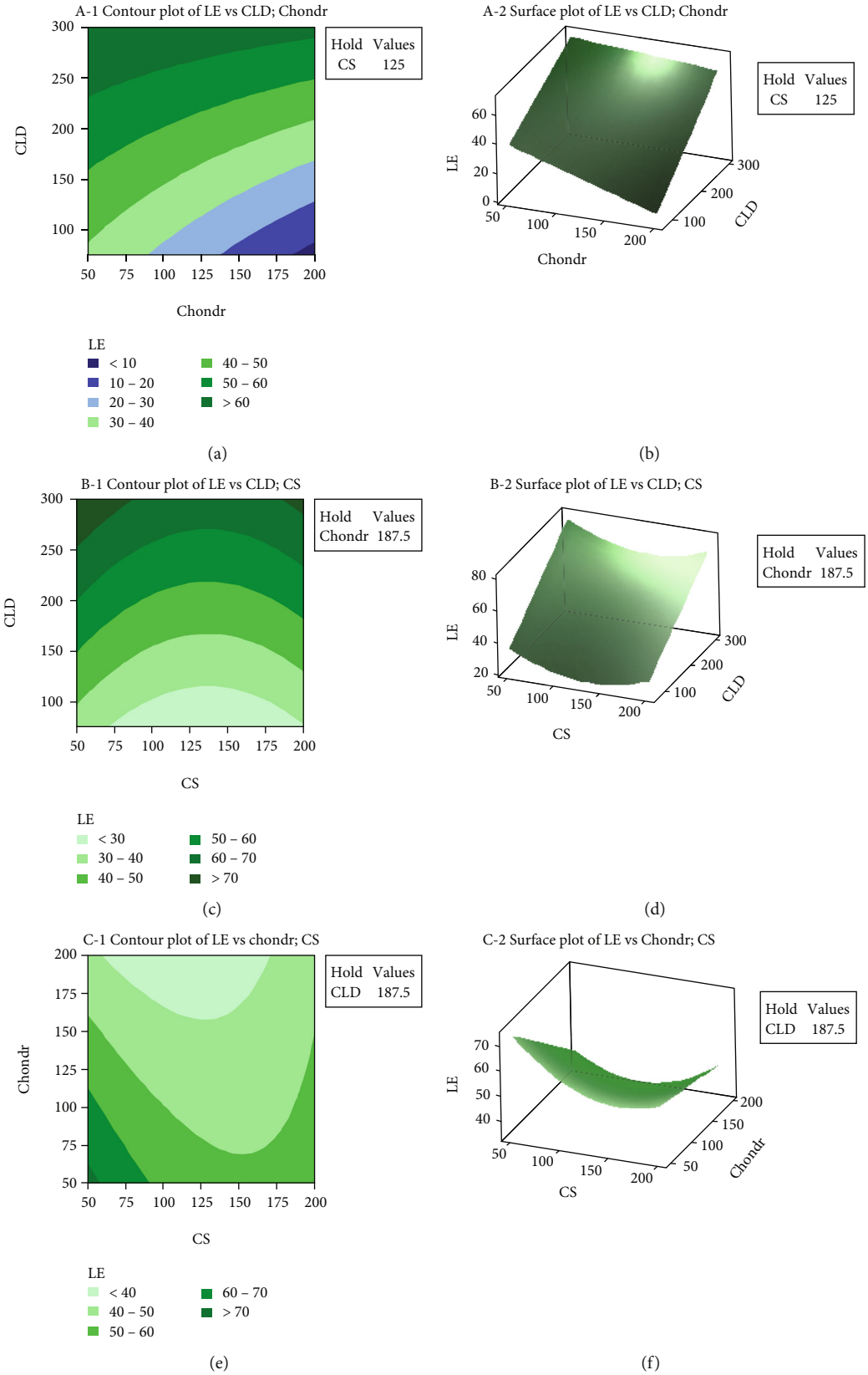

Figure 6: Contour plots and surface plots of %LE.

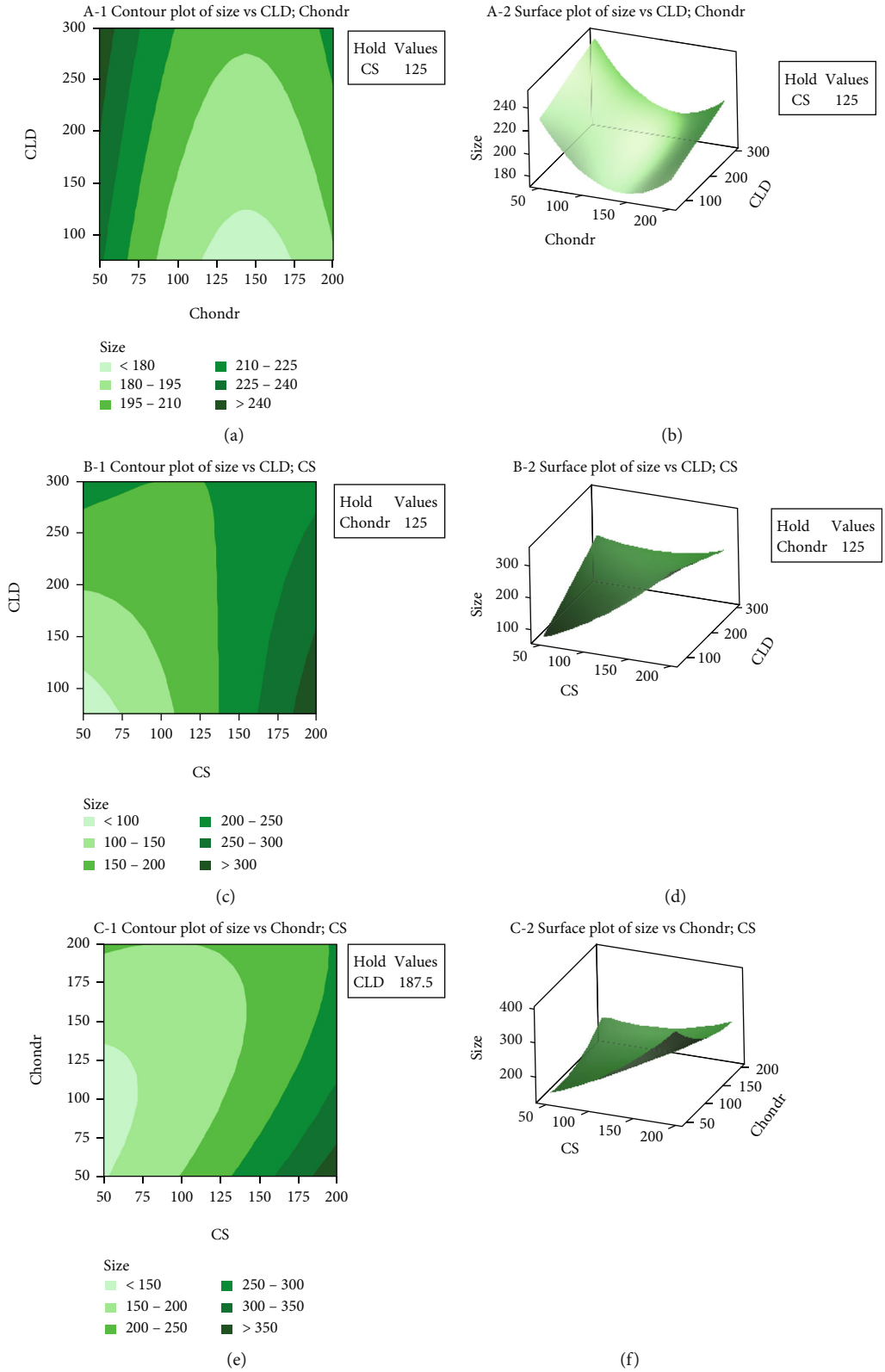

Figure 7: The contour plots and surface plots of size against different factors.

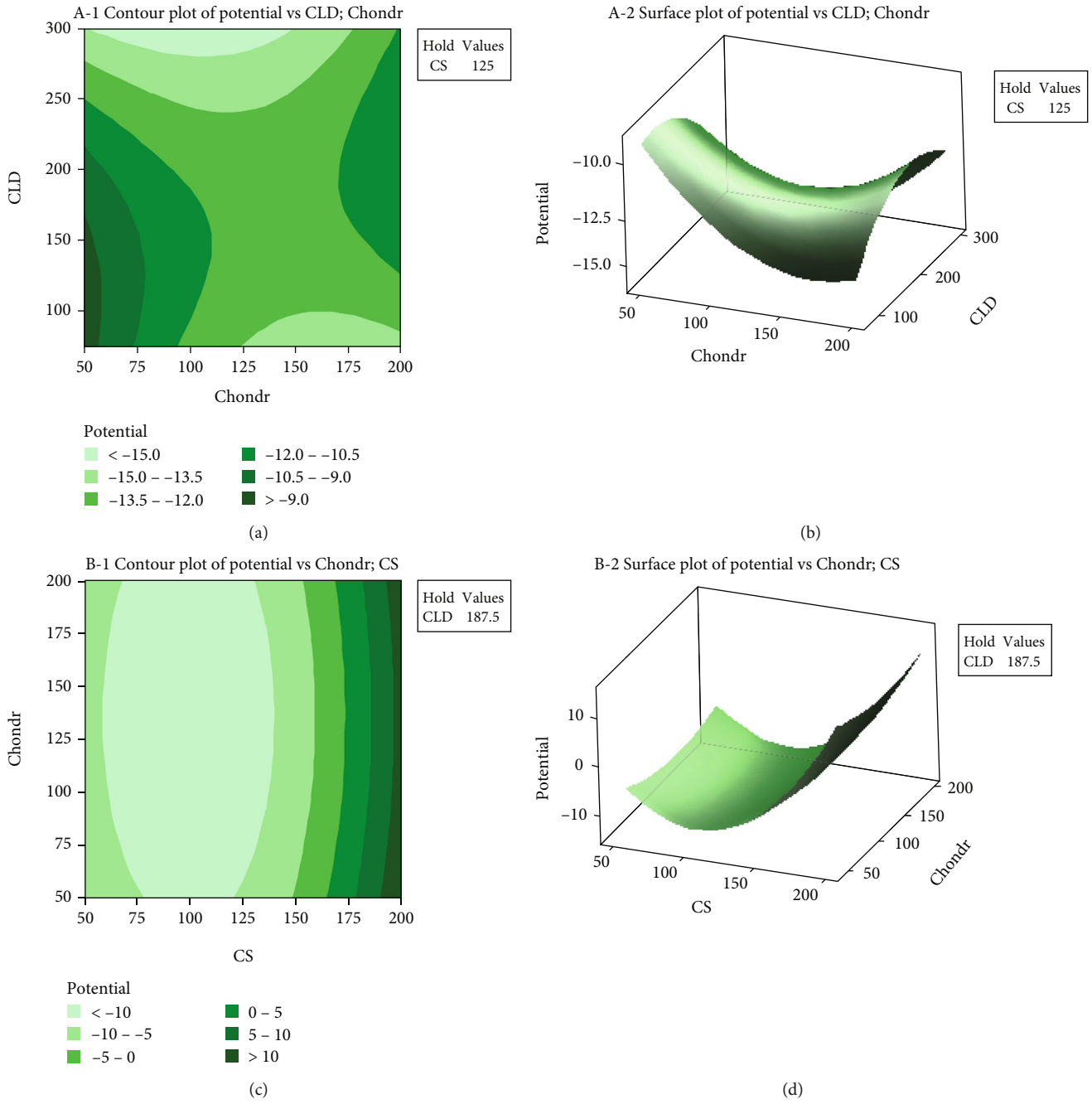

Figure 8: Continued.

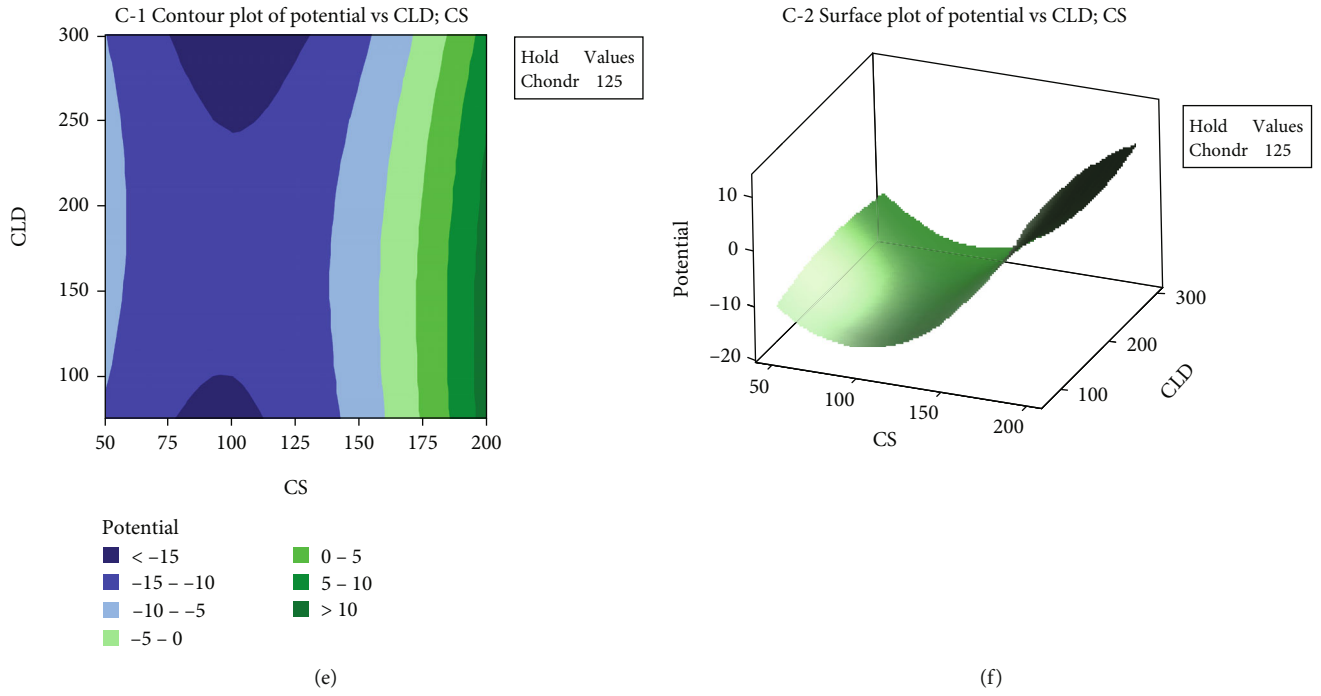

(e) (f)

Figure 8: The contour plot and surface plot of zeta potential against different factors.

Table 5: Comparison of the observed and predicted values of the response variables of optimized formulation.

Concentrations	Experimental response	Predicted values	Observed values	Bias (%)
CS = 200 mg Chondro = 138 mg CLD = 254 mg	LE (%)	64.1	61.2	-4.5
	Particle size (nm)	271.0	253.4	-6.5
	Zeta potential (mV)	11.7	11.3	-3.4
CS = 128 mg Chondro = 138 mg CLD = 254 mg	LE (%)	56.0	52.4	-6.4
	Particle size (nm)	220.0	220.7	0.3
	Zeta potential (mV)	-11.3	-10.9	-3.5
CS = 160 mg Chondro = 112 mg CLD = 149 mg	LE (%)	35.0	39.0	11.4
	Particle size (nm)	263.4	259.1	-1.6
	Zeta potential (mV)	-13.9	-14.5	5.4

Bias was calculated as (observed value – predicted value/predicted value) × 100%.

Figure 7(a) shows the contour plot of size against the Chondro and CLD. The smallest values of particle size are at the bottom of the plot, which corresponds with 50 mg of CLD, and Chondro varies from 115 mg to 175 mg; the surface is minimum (Figure 7(b)).

In Figure 7(c), the contour plot shows that the minimum particle size occurs at low concentrations of CS and CLD; the surface is minimum (Figure 7(d)). In addition, Figure 7(e) shows the contour plot of size against the Chondro and CS. The smallest values of particle size are at the bottom left of the plot, which corresponds with 50 mg of CS, and Chondro and varies from 50 mg to 175 mg; the surface is minimum (Figure 7(f)).

Figures 8(a) and 8(b) shows the contour plot of zeta potential against the Chondro and CLD. The -15 mV zeta potential can be collected at Chondro concentration range of 50-200 mg and CLD at 300 mg. The -9 mV zeta potential can be collected at Chondro concentration below 60 mg and CLD ranging between 50 and 160 mg.

Figure 8(c) shows that the zeta potential was dependent on CS and Chondro. When CS was more than 190 mg and at the same time the Chondro was between 50 and 200 mg, the zeta potential was found to be +10 mV (Figure 8(d)). In addition, when CS variables were in the range 75-125 mg and the Chondro was between 50 and 200 mg, the zeta potential was found to be -10 mV (Figure 8(d)). The contour of CS vs. CLD concentrations is shown in Figure 8(e). When CS variables were between 50 and 190 mg and at same time the CLD was between 50 and 300 mg, the zeta potential was found to be -15 mV (Figures 8(e) and 8(f)). Finally, when the CS concentrations were more than 160 mg, they produced a positive value of zeta potential.

4.9. Prediction, Optimization, and Validation of Three Models. Taking into account the main factors in our work (A, B, and C) and their combinations (A ∗ A, B ∗ B, C ∗ C, A ∗ B, A ∗ C, and B ∗ C), a general equation can be obtained with regard to the real values by a response surface method. For predicting %LE, particle size, and zeta potential, the following equations were derived:

$$\begin{aligned}
\%\text{LE} &= 91.21 - 0.627\,\text{CS} - 0.3962\,\text{Chondro} \\
&\quad + 0.1023\,\text{CLD} + 0.001816\,\text{CS} * \text{CS} \\
&\quad + 0.001038\,\text{CS} * \text{Chondro} \\
&\quad + 0.000733\,\text{Chondro} * \text{CLD}. \\
\text{Particle size} &= -56.3 + 2.170\,\text{CS} - 0.661\,\text{Chondro} \\
&\quad + 1.0236\,\text{CLD} + 0.00496\,\text{CS} * \text{CS} \\
&\quad + 0.00601\,\text{Chondro} * \text{Chondro} \\
&\quad - 0.008586\,\text{CS} * \text{Chondro}0.007388\,\text{CS} \\
&\quad * \text{CLD}. \\
\text{Zeta potential} &= 16.44 - 0.4745\,\text{CS} - 0.1626\,\text{Chondro} \\
&\quad + 0.0443\,\text{CLD} + 0.002555\,\text{CS} * \text{CS} \\
&\quad + 0.000421\,\text{Chondr} * \text{Chondr} \\
&\quad - 0.000173\,\text{CLD} * \text{CLD} - 0.000174\,\text{CS} \\
&\quad * \text{CLD} + 0.000259\,\text{Chondr} * \text{CLD}.
\end{aligned} \tag{8}$$

According to our criteria for higher %LE (88.86%), the concentrations under canonical analysis were selected at 50 mg, 50 mg, and 300 mg, of CS, Chondro, and CLD, respectively. In addition, to prepare nanoparticles with a size of 64 nm, 50 mg CS, 91 mg Chondro, and 75 mg CLD were used. Furthermore, the zeta potential with -17 mV value can be obtained by using 103.3 mg CS, 101.5 mg Chondro, and 300 mg CLD.

A bias formula under optimized factors was applied to compare with the predicted values. As shown in Table 5, the bias was around −4.5%, −6.5%, and 3.4% for the first formula (CS = 200 mg, Chondro = 138 mg, and CLD = 254 mg). In addition, the bias was around −6.4%, 0.3%, and -3.5% for the second formula (CS = 128 mg, Chondro = 138 mg, and CLD = 254 mg) and around 11.4%, -1.6%, and 15.4% for the third formula (CS = 160 mg, Chondro = 112 mg, and CLD = 149 mg), respectively. These results indicate the validity of the generated models with no statistically significant difference and good correlation between predicted and experimental values.

The zeta potential (mV) of nanocarriers represents the surface charge. It depends on the dispersing medium as well as the composition of the particles. The nanoparticles that possess zeta potentials between +30 mV and −30 mV are considered a stable system that prevents nanoparticle aggregation. From Table 5, the observed zeta potential values of nanocomposites are 11.3, -10.9, and -14.5 mV. These values indicate that the nanocomposites were stable.

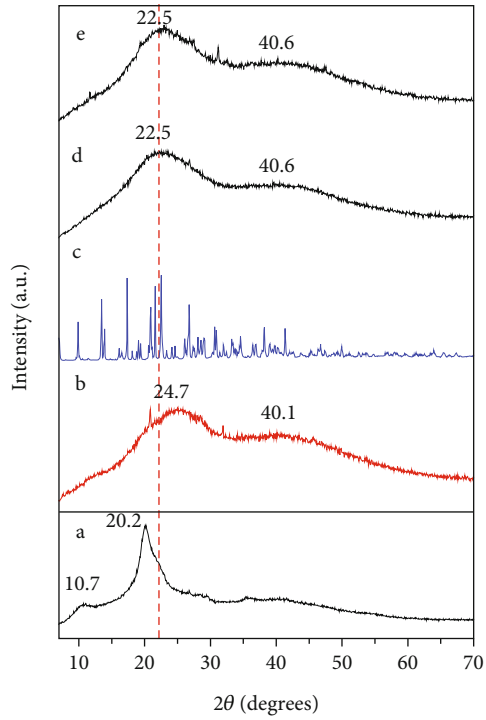

Figure 9: Powder X-ray diffraction patterns of the CS (a), Chondro (b), CLD (c), CS-Chondro (d), and CS-Chondro-CLD nanocomposites (e).

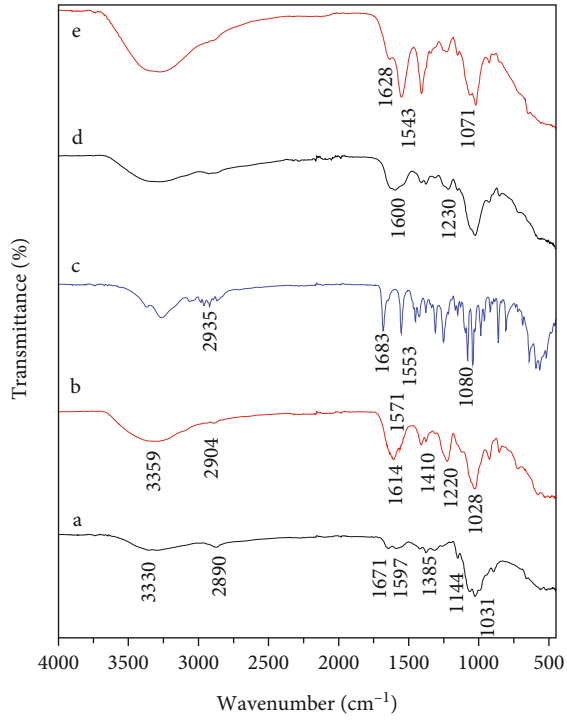

Figure 10: FT-IR spectrum of CS (a), Chondro (b), CLD (c), CS-Chondro (d), and CS-Chondro-CLD nanocomposites (e).

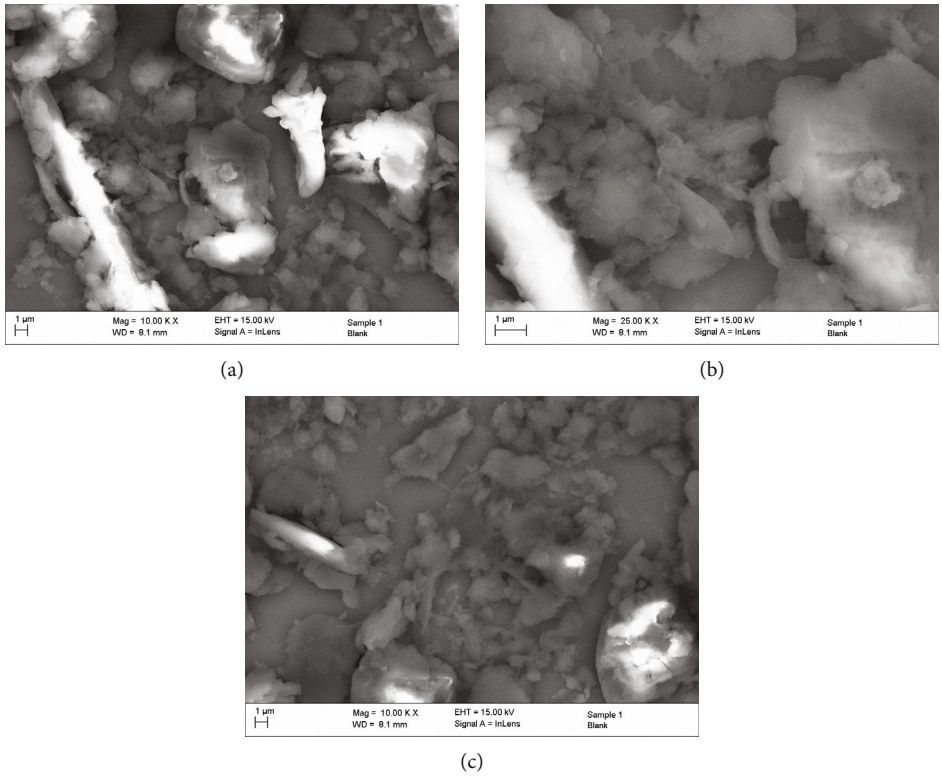

Figure 11: SEM images of Chondro-CS (a, b) and Chondro-CS-CLD (c).

5. Characterization of Formulations

5.1. X-Ray Diffraction (XRD). Figures 9 (a), (b), (c), (d), and (e) shows the XRD patterns of CS, Chondro, CLD, CS-Chondro, and CS-Chondro-CLD nanocomposites, respectively. From Figure 9(a), CS showed strong diffraction peaks at $2\theta = 10.7$ and 20.2°, indicating a high degree of crystallinity [41, 42].

Diffraction broad bands similar to Chondro were seen for CS-Chondro and CS-Chondro-CLD due to amorphous behavior of the polymer. The diffraction peaks of Chondro were observed at 24.7 and 40.1° (Figure 9(b)), whereas the diffraction peaks with maximum intensity were observed at 22.5 for CS-Chondro and CS-Chondro-CLD as seen in Figures 9(d) and (e). These diffraction peaks in Chondro, CS-Chondro, and CS-Chondro-CLD were very broad which is indicative of their highly amorphous nature with low crystallinity [43].

5.2. Infrared Spectroscopy (FTIR). The IR spectra of CS (a), Chondro (b), CLD (c), CS-Chondro (d), and CS-Chondro-CLD nanocomposites (e), respectively, are shown in Figure 10. IR spectrum of CS showed vibration at 3330 cm^{-1} due to overlapped –OH and N–H stretching; the C–H stretching of CH_3 or CH_2 groups of CS is at 2890 cm^{-1}. The peaks at 1671 and 1597 cm^{-1} correspond to the amide bonds and NH_2 group, respectively. The peak at 1385 cm^{-1} due to stretching of C=N bond and the stretching of C–O bond are shown at 1,079 and 1,030 cm^{-1} [44].

The IR spectrum of Chondro in Figure 10(b) showed the –OH and N–H stretching at 3359 cm^{-1}. The peak at 2904 cm^{-1} was due to C–H stretching of CH_3 or CH_2 groups. The peak at 1614 cm^{-1} was due to the amide bands, whereas the peaks at 1413 and 1380 cm^{-1} are due to the C–O stretch vibration, indicating the presence of a free carboxyl group. The peak at 1220 cm^{-1} was due to the stretching of S=O bond of SO_4^{2-} [44].

The IR spectrum of CS-Chondro is shown in Figure 10(c). The peak at 1671 cm^{-1} for amide in CS was shifted to 1600 cm^{-1}, whereas the peak of NH_2 group disappeared, and this leads to cross-linking of NH_2 of CS with Chondro [44]. The peak at 1220 cm^{-1} of S=O turned weaker and shifted to 1230 cm^{-1}, which indicates cross-linking of SO_4^{2-} group of CS with Chondro.

The FT-IR spectrum of CLD in Figure 10(c) showed characteristics of peaks at 1683 cm^{-1} (C=O stretching), 1080 cm^{-1} (C-O stretching), 1553 cm^{-1} (C=C stretching), and 2935 cm^{-1}(C-H stretching) [45].

Comparing the FT-IR spectrum of CS-Chondro-CLD in Figure 10(e) with the FT-IR spectrum of the CS-Chondro in Figure 10(d), two specific peaks of CLD can be seen to have appeared at 1683 $cm^{-1}$and 1553 cm^{-1}, indicating the incorporation of CLD into the CS-Chondro-CLD.

5.3. Scanning Electron Microscopy. SEM images are widely used to examine the surface morphology of polysaccharides [46]. The morphological analysis of Chondro-CS and Chondro-CS-CLD in this study was carried out using SEM.

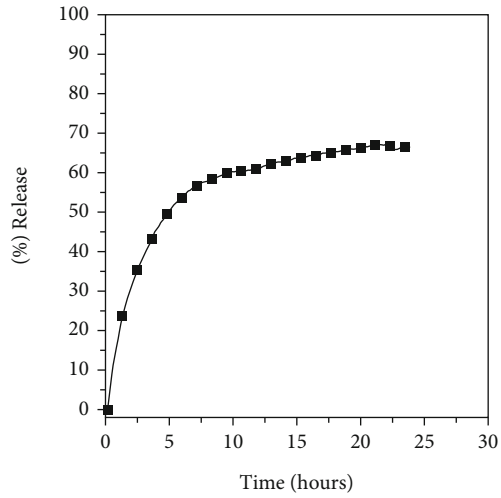

Figure 12: *In vitro* release profiles of CLD from nanocomposite at pH 7.4.

Figure 11 shows the SEM images of Chondro-CS and Chondro-CS-CLD with magnifications of 10000x and 25000x. It could be seen that the morphological properties of both Chondro-CS and Chondro-CS-CLD were similar (Figure 11(a)–11(c)). The Chondro-CS and Chondro-CS-CLD had a smooth homogeneous surface with lots of particle layers stacked together.

5.4. In Vitro Release Study. The release profiles of CLD from the optimized sample at pH 7.4 are illustrated in Figure 12.

It was noticed that the release rate of CLD at pH 7.4 was significantly very slow, where it started after 1 hour. This result can be explained based on the swelling term [47, 48]. The last results suggest that the CLD release profile was prominently prolonged by the encapsulation.

6. Conclusion

The aim of this work was to study the factors affecting the %LE, zeta potential, and particle size using response surface methodology model. The results indicated that for %LE, the square (Chondro ∗ Chondro and CLD ∗ CLD) and two-way interaction (CS ∗ CLD) was excluded from the final equation, whereas at size response, two-way interaction (Chondro ∗ CLD) only was excluded from the final equation. In addition, at zeta potential response, two-way interaction (CS ∗ Chondro) was excluded from the final equation. The developed multiple linear regression models provided the best fits to the data set. The XRD spectra of nanocomposites showed amorphous forms. The FT-IR data shows the functional group of CLD in nanocomposites, indicating incorporation of CLD into the nanocomposites. In addition, the prepared formulation shows sustained release, which may increase the chance for the patient to respond to the medication, since formulations are generally characterized by one daily given dose.

Data Availability

The original data can collected from Prof Samer AlAli by contact in his email sameralali72@yahoo.com or samer.alali@iu.edu.jo.

Conflicts of Interest

The authors report no conflicts of interest in this work.

Acknowledgments

The authors would like to thank the Faculty of Pharmacy at Isra University for provided funding for this research 2017/2018/19 (6/9/2018). Furthermore, the authors would like to acknowledge the Institute of Functional Nanosystems for the permission to use their advanced facilities in UIM University (Germany).

References

[1] D. K. Robinson, A. Rip, and V. Mangematin, "Technological agglomeration and the emergence of clusters and networks in nanotechnology," *Research Policy*, vol. 36, no. 6, pp. 871–879, 2007.

[2] P. Christian, F. von der Kammer, M. Baalousha, and T. Hofmann, "Nanoparticles: structure, properties, preparation and behaviour in environmental media," *Ecotoxicology*, vol. 17, no. 5, pp. 326–343, 2008.

[3] P. Homayonpour, H. Jalali, N. Shariatifar, and M. Amanlou, "Effects of nano-chitosan coatings incorporating with free /nano-encapsulated cumin (_Cuminum cyminum_ L.) essential oil on quality characteristics of sardine fillet," *International Journal of Food Microbiology*, vol. 341, article 109047, 2021.

[4] B. Vigani, S. Rossi, G. Sandri, M. C. Bonferoni, C. M. Caramella, and F. Ferrari, "Hyaluronic acid and chitosan-based nanosystems: a new dressing generation for wound care," *Expert Opinion on Drug Delivery*, vol. 16, no. 7, pp. 715–740, 2019.

[5] M. Yeganeh, E. Charkhloo, H. R. Sobhi, A. Esrafili, and M. Gholami, "Photocatalytic processes associated with degradation of pesticides in aqueous solutions: systematic review and _meta_ -analysis," *Chemical Engineering Journal*, vol. 428, article 130081, 2022.

[6] R. Noroozi, M. Gholami, M. Farzadkia, and A. Jonidi Jafari, "Degradation of ciprofloxacin by $CuFe_2O_4$/GO activated PMS process in aqueous solution: performance, mechanism and degradation pathway," *International Journal of Environmental Analytical Chemistry*, vol. 102, no. 1, pp. 174–195, 2022.

[7] N. M. Mahmoodi and M. Arami, "Modeling and sensitivity analysis of dyes adsorption onto natural adsorbent from colored textile wastewater," *Journal of Applied Polymer Science*, vol. 109, no. 6, pp. 4043–4048, 2008.

[8] D. Asefi, N. M. Mahmoodi, and M. Arami, "Effect of nonionic co-surfactants on corrosion inhibition effect of cationic gemini surfactant," *Colloids and Surfaces A: Physicochemical and Engineering Aspects*, vol. 355, no. 1-3, pp. 183–186, 2010.

[9] S. Bhatia and S. Bhatia, "Nanoparticles types, classification, characterization, fabrication methods and drug delivery applications," in *Natural Polymer Drug Delivery Systems*, pp. 33–93, Springer, 2016.

[10] B. Mishra, B. B. Patel, and S. Tiwari, "Colloidal nanocarriers: a review on formulation technology, types and applications toward targeted drug delivery," *Nanomedicine: Nanotechnology, Biology and Medicine*, vol. 6, no. 1, pp. 9–24, 2010.

[11] C. Dussaubat, J. L. Brunet, M. Higes et al., "Gut pathology and responses to the microsporidium Nosema ceranae in the honey bee Apis mellifera," *PLoS One*, vol. 7, no. 5, article e37017, 2012.

[12] J. N. Hathcock and A. Shao, "Risk assessment for glucosamine and chondroitin sulfate," *Regulatory Toxicology and Pharmacology*, vol. 47, no. 1, pp. 78–83, 2007.

[13] O. Bukalo, M. Schachner, and A. Dityatev, "Modification of extracellular matrix by enzymatic removal of chondroitin sulfate and by lack of tenascin-R differentially affects several forms of synaptic plasticity in the hippocampus," *Neuroscience*, vol. 104, no. 2, pp. 359–369, 2001.

[14] A.-M. Anton, I. Rau, F. Kajzar, A. M. Simion, and C. Simion, "Third order nonlinear optical properties of DNA-based biopolymers thin films doped with selected natural chromophores," *Optical Materials*, vol. 88, pp. 181–186, 2019.

[15] P. Homayonpour, H. Jalali, N. Shariatifar, and M. Amanlou, "Performance investigation of Zeolitic Imidazolate Framework - 8 (ZIF-8) in the removal of trichloroethylene from aqueous solutions," *Microchemical Journal*, vol. 150, article 104185, 2019.

[16] R. Duncan and J. Kopeček, "Soluble synthetic polymers as potential drug carriers," in *Polymers in Medicine*, Springer, Berlin, Heidelberg, 1984.

[17] M. Smieja, "Current indications for the use of clindamycin: a critical review," *Canadian Journal of Infectious Diseases and Medical Microbiology*, vol. 9, 28 pages, 1998.

[18] M. Seminario-Amez, J. López-López, A. Estrugo-Devesa, R. Ayuso-Montero, and E. Jané-Salas, "Probiotics and oral health: a systematic review," *Medicina Oral, Patología Oral y Cirugía Bucal*, vol. 22, article e282, e288 pages, 2017.

[19] M. J. Kasten, "Clindamycin, metronidazole, and chloramphenicol," *Mayo Clinic Proceedings*, vol. 74, no. 8, pp. 825–833, 1999.

[20] M. Abbaspour, B. S. Makhmalzadeh, Z. Arastoo, A. Jahangiri, and R. Shiralipour, "Effect of anionic polymers on drug loading and release from clindamycin phosphate solid lipid nanoparticles," *Tropical Journal of Pharmaceutical Research*, vol. 12, no. 4, pp. 477–482, 2013.

[21] A. A. Abdellatif and H. M. Tawfeek, "Transfersomal nanoparticles for enhanced transdermal delivery of clindamycin," *AAPS PharmSciTech*, vol. 17, no. 5, pp. 1067–1074, 2016.

[22] P. R. Rauta, N. M. das, D. Nayak, S. Ashe, and B. Nayak, "Enhanced efficacy of clindamycin hydrochloride encapsulated in PLA/PLGA based nanoparticle system for oral delivery," *IET Nanobiotechnology*, vol. 10, no. 4, pp. 254–261, 2016.

[23] M. Kilicarslan, M. Ilhan, O. Inal, and K. Orhan, "Preparation and evaluation of clindamycin phosphate loaded chitosan/alginate polyelectrolyte complex film as mucoadhesive drug delivery system for periodontal therapy," *European Journal of Pharmaceutical Sciences*, vol. 123, pp. 441–451, 2018.

[24] O. Borges, G. Borchard, J. C. Verhoef, A. de Sousa, and H. E. Junginger, "Preparation of coated nanoparticles for a new mucosal vaccine delivery system," *International Journal of Pharmaceutics*, vol. 299, no. 1-2, pp. 155–166, 2005.

[25] M. K. Yeh, K. M. Cheng, C. S. Hu, Y. C. Huang, and J. J. Young, "Novel protein-loaded chondroitin sulfate-chitosan nanoparticles: preparation and characterization," *Acta Biomaterialia*, vol. 7, no. 10, pp. 3804–3812, 2011.

[26] T. A. Abdullah, N. J. Ibrahim, and M. H. Warsi, "Chondroitin sulfate-chitosan nanoparticles for ocular delivery of bromfenac sodium: improved permeation, retention, and penetration," *International journal of pharmaceutical investigation*, vol. 6, no. 2, pp. 96–105, 2016.

[27] B. Saifullah, M. Z. Hussein, S. H. Hussein-Al-Ali, P. Arulselvan, and S. Fakurazi, "Antituberculosis nanodelivery system with controlled-release properties based on para-amino salicylate–zinc aluminum-layered double-hydroxide nanocomposites," *Drug Design, Development and Therapy*, vol. 7, p. 1365, 2013.

[28] M. J. Anderson, "Distance-based tests for homogeneity of multivariate dispersions," *Biometrics*, vol. 62, no. 1, pp. 245–253, 2006.

[29] G. J. McLachlan, "Mahalanobis distance," *Resonance*, vol. 4, no. 6, pp. 20–26, 1999.

[30] L. Murray, H. Nguyen, Y. F. Lee, M. D. Remmenga, and D. W. Smith, *Variance Inflation Factors in Regression Models with Dummy Variables*, 2012.

[31] S. Sinharay, "An overview of statistics in education," in *International Encyclopedia of Education (Third Edition)*, P. Peterson, E. Baker, and B. McGaw, Eds., pp. 1–11, Elsevier, Oxford, 2010.

[32] K. Nishimura, S. I. Nishimura, H. Seo, N. Nishi, S. Tokura, and I. Azuma, "Macrophage activation with multi-porous beads prepared from partially deacetylated chitin," *Journal of Biomedical Materials Research Part A*, vol. 20, no. 9, pp. 1359–1372, 1986.

[33] A. Jain and S. K. Jain, "Formulation and optimization of temozolomide nanoparticles by 3 factor 2 level factorial design," *Biomatter*, vol. 3, no. 2, article e25102, 2013.

[34] G. Khairnar, J. Naik, and V. Mokale, "A statistical study on the development of micro particulate sustained drug delivery system for losartan potassium by 3^2 factorial design approach," *Bulletin of Faculty of Pharmacy, Cairo University*, vol. 55, no. 1, pp. 19–29, 2017.

[35] F. J. Massey, "The Kolmogorov-Smirnov test for goodness of fit," *Journal of the American Statistical Association*, vol. 46, no. 253, pp. 68–78, 1951.

[36] G. Fasano and A. Franceschini, "A multidimensional version of the Kolmogorov–Smirnov test," *Monthly Notices of the Royal Astronomical Society*, vol. 225, no. 1, pp. 155–170, 1987.

[37] A. Justel, D. Peña, and R. Zamar, "A multivariate Kolmogorov-Smirnov test of goodness of fit," *Statistics & Probability Letters*, vol. 35, no. 3, pp. 251–259, 1997.

[38] P. O'Connor and A. Kleyner, *Practical reliability engineering*, John Wiley & Sons, 2012.

[39] R. D'Agostino and M. Stephens, *Tests for Normal Distribution in Goodness-Of-Fit Techniques, Statistics: Textbooks and Monographs*, R. B. D'Agostino and M. A. Stephens, Eds., Dekker, New York, 1986.

[40] "Quick and easy analysis of Unreplicated factorials," *Technometrics*, vol. 31, no. 4, pp. 469–473, 1989.

[41] L. Qi, Z. Xu, X. Jiang, C. Hu, and X. Zou, "Preparation and antibacterial activity of chitosan nanoparticles," *Carbohydrate Research*, vol. 339, no. 16, pp. 2693–2700, 2004.

[42] C. Radhakumary, P. D. Nair, S. Mathew, and C. R. Nair, "Biopolymer composite of chitosan and methyl methacrylate for

medical applications," *Biomaterials and Artificial Organs*, vol. 18, no. 2, pp. 117–124, 2005.

[43] J. Venkatesan, R. Pallela, I. Bhatnagar, and S. K. Kim, "Chitosan-amylopectin/hydroxyapatite and chitosan-chondroitin sulphate/hydroxyapatite composite scaffolds for bone tissue engineering," *International Journal of Biological Macromolecules*, vol. 51, no. 5, pp. 1033–1042, 2012.

[44] J. R. Amrutkar and S. G. Gattani, "Chitosan–chondroitin sulfate based matrix tablets for colon specific delivery of indomethacin," *AAPS PharmSciTech*, vol. 10, no. 2, pp. 670–677, 2009.

[45] P. Patel and P. Patel, "Formulation and evaluation of clindamycin HCL in situ gel for vaginal application," *International journal of pharmaceutical investigation*, vol. 5, no. 1, pp. 50–56, 2015.

[46] D. A. Brant, "Novel approaches to the analysis of polysaccharide structures," *Current Opinion in Structural Biology*, vol. 9, no. 5, pp. 556–562, 1999.

[47] C. S. Nunes, K. B. Rufato, P. R. Souza et al., "Chitosan/chondroitin sulfate hydrogels prepared in [Hmim][HSO_4] ionic liquid," *Carbohydrate Polymers*, vol. 170, pp. 99–106, 2017.

[48] S. Nanda, N. Sood, B. V. K. Reddy, and T. S. Markandeywar, "Preparation and characterization of poly(vinyl alcohol)-chondroitin sulphate hydrogel as scaffolds for articular cartilage regeneration," *Indian Journal of Materials Science*, vol. 2013, Article ID 516021, 8 pages, 2013.